Tellus (1998), 50B, 1–24
Printed in UK – all rights reserved

TELLUS
ISSN 0280–6509

Seasonal and interannual variations of atmospheric CO_2 and climate

By MICHAEL D. DETTINGER*[1] and MICHAEL GHIL[2], [1]*US Geological Survey, 5735 Kearny Villa Road, Suite O, San Diego, California 92123 USA*, [2]*Department of Atmospheric Sciences and Institute of Geophysics and Planetary Physics, University of California, Los Angeles, California 90095 USA*

(Manuscript received 6 September 1996; in final form 14 August 1997)

ABSTRACT

Interannual variations of atmospheric CO_2 concentrations at Mauna Loa are almost masked by the seasonal cycle and a strong trend; at the South Pole, the seasonal cycle is small and is almost lost in the trend and interannual variations. Singular-spectrum analysis (SSA) is used here to isolate and reconstruct interannual signals at both sites and to visualize recent decadal changes in the amplitude and phase of the seasonal cycle. Analysis of the Mauna Loa CO_2 series illustrates a hastening of the CO_2 seasonal cycle, a close temporal relation between Northern Hemisphere (NH) mean temperature trends and the amplitude of the seasonal CO_2 cycle, and tentative ties between the latter and seasonality changes in temperature over the NH continents. Variations of the seasonal CO_2 cycle at the South Pole differ from those at Mauna Loa: it is phase changes of the seasonal cycle at the South Pole, rather than amplitude changes, that parallel hemispheric and global temperature trends. The seasonal CO_2 cycles exhibit earlier occurrences of the seasons by 7 days at Mauna Loa and 18 days at the South Pole. Interannual CO_2 variations are shared at the two locations, appear to respond to tropical processes, and can be decomposed mostly into two periodicities, around $(3 \text{ years})^{-1}$ and $(4 \text{ years})^{-1}$, respectively. Joint SSA analyses of CO_2 concentrations and tropical climate indices isolate a shared mode with a quasi-triennial (QT) period in which the CO_2 and sea-surface temperature (SST) participation are in phase opposition. The other shared mode has a quasi-quadrennial (QQ) period and CO_2 variations are in phase with the corresponding tropical SST variations throughout the tropics. Together these interannual modes exhibit a mean lag between tropical SSTs and CO_2 variations of about 6–8 months, with SST leading. Analysis of the QT and QQ signals in global gridded SSTs, joint SSA of CO_2 and $\delta^{13}C$ isotopic ratios, and SSA of CO_2 and NH-land temperatures indicate that the QT variations in CO_2 mostly reflect upwelling variations in the eastern tropical Pacific. QQ variations are dominated by the CO_2 signature of terrestrial-ecosystem response to global QQ climate variations. Climate variations associated with these two interannual components of tropical variability have very different effects on global climate and, especially, on terrestrial ecosystems and the carbon cycle.

1. Introduction

Atmospheric CO_2 concentrations at Mauna Loa and the South Pole have been monitored regularly since about 1958 and 1965, respectively. Concentrations at other sites around the globe have been monitored for shorter periods. All the CO_2 time series show a well-known and dramatic global increase that is ascribed mostly to fossil-fuel combustion and, less so, to land-use changes and deforestation (Sundquist, 1993). In addition to this trend, CO_2 concentrations generally have seasonal cycles that vary from place to place, as well as modest interannual fluctuations (Keeling et al., 1989; Lambert et al., 1995). Seasonal cycles

* Corresponding author.
email: mddettin@usgs.gov

in CO_2 concentrations are ascribed to seasonal changes in terrestrial ecosystems and, less so, marine CO_2 uptake (Ciais et al., 1995); they have increased in amplitude in recent decades, perhaps as a reflection of increasing mean concentrations or mean global-scale temperatures (Okamoto et al., 1995; Keeling et al., 1996; Myneni et al., 1997). Interannual fluctuations are attributed to changes in upwelling of CO_2-rich ocean waters in the tropics and changes in terrestrial ecosystems associated with regional climate expressions of El Niño and volcanic eruptions (Siegenthaler, 1990; Sarmiento, 1993; Keeling et al., 1995).

Understanding these small CO_2 fluctuations should help provide insights into the mechanisms controlling atmospheric CO_2 concentrations and the partitioning of CO_2 changes between terrestrial and marine sources and sinks, as well as — according to the present analysis — into the relative effects of tropical and extratropical climate variations on global ecosystems. On interannual time scales in particular, spectral analyses of climate indices in both the tropics and extratropics have yielded a number of narrow-band signals (Ghil and Vautard, 1991; Mann and Park, 1994; Dettinger et al., 1995a). Such relatively regular signals facilitate the exploration of their causal mechanisms. In the tropics, for instance, the presence of quasi-biennial (QB), quasi-quadrennial (QQ), and possibly 4/3-year signals (Rasmusson et al., 1990; Keppenne and Ghil, 1992; Jiang et al., 1995) has led to the formulation of a mechanism that involves the nonlinear interaction between the seasonal cycle and an intrinsic El Niño-Southern Oscillation (ENSO) instability with a period of 2–3 years (Chang et al., 1994; Jin et al., 1994; Tziperman et al., 1994) to explain the several narrow- and broad-band interannual frequencies of ENSO. It is our premise here that a similar decomposition of the interannual CO_2 fluctuations, although they are small, into narrow-band signals can shed further light on feedback networks within the complex physico-biogeochemical climate-CO_2 system.

The seasonal and interannual variations of CO_2 concentrations studied here are the result of imbalances between large carbon sources and sinks on land and sea. Photosynthesis on land removes CO_2 from the atmosphere whereas respiration and combustion return CO_2 to the atmosphere. The terrestrial biosphere is a source of atmospheric CO_2 in winter and a sink in summer. On average, the oceans constitute a CO_2 sink (Siegenthaler and Sarmiento, 1993) but that average includes large regional and interannual differences. Tropical-ocean surface waters typically are warm and have low CO_2 solubility, but, in the eastern tropical Pacific, are cool and CO_2 rich so that CO_2 generally is released to the atmosphere from the tropical oceans (with notable exceptions to be discussed). Higher latitude waters are cooler, have higher CO_2 solubility, and thus are CO_2 sinks.

On seasonal time scales, CO_2 variations mostly reflect the metabolic activity of terrestrial plants and soils (Bacastow et al., 1985; Nemry et al., 1996), especially in the Northern Hemisphere (NH). In summer, photosynthesis dominates and decreases CO_2 concentrations whereas, in winter, respiration dominates and increases CO_2. Regardless of season, however, the contribution of the terrestrial biosphere is always a difference between photosynthetic sinks and respiration sources. Photosynthesis by land plants increases with temperature but not as much, typically, as do plant and soil respiration (Keeling et al., 1996). Thus warmer climates and longer growing seasons can lead to increased CO_2 concentrations. Changes in the seasonal imbalances are such that a warmer climate overall also can increase the amplitude of the seasonal CO_2 cycle. In contrast, Knorr and Heimann (1995) find that water availability has limited net impact on the CO_2 seasonal cycle at mid-to-high latitudes. Ocean uptake of CO_2 varies with seasons (being a stronger net sink in summer when atmospheric CO_2 partial pressures are highest) but these variations are smaller than the terrestrial contributions (Ciais et al., 1995).

On interannual time scales, marine and terrestrial CO_2 balances are both of crucial importance. Warmer-than-normal continental temperatures can increase the rate of CO_2 release from soils (Trumbore et al., 1996; Knorr and Heimann, 1995). Droughts can limit photosynthesis rates and ultimately may increase wildfires, thus tipping terrestrial balances toward increased respiration and higher atmospheric CO_2 concentrations (Siegenthaler and Sarmiento, 1993). Consequently, increases in terrestrial CO_2 sources during El Niños have been attributed to overall continental warming and (mostly tropical) droughts associated with the warm-tropical episodes

(Siegenthaler, 1990; Keeling et al., 1995, 1996); opposite effects are attributed to La Niñas. Warmer-than-normal surface waters dominate the tropical Pacific during El Niños and displace the cooler but CO_2-rich waters that typically upwell from the Equatorial Undercurrent beneath the eastern equatorial Pacific (Murray et al., 1994). The effect of this displacement is to reduce or even reverse CO_2 release by the tropical oceans and to increase net global-oceanic uptake of CO_2 (Francey et al., 1995). As a consequence, the oceans are a stronger CO_2 sink, overall, during El Niños and thus, when tropical SSTs are warm, the oceans contribute to lower CO_2 concentrations. Usually, however, the increases in terrestrial sources of CO_2 during El Niños dominate and CO_2 concentrations increase overall during the warm episodes. In this paper, we will demonstrate that the balance between these marine and terrestrial influences on CO_2 concentration vary within the ENSO spectral band of tropical variability depending on the strength and spatial extent of the ENSO climate modes involved.

We clarify here some of these narrow-band climate-CO_2 relations by application of a data-adaptive spectral-analysis method, called singular-spectrum analysis (SSA; see Section 2), to the Mauna Loa and South Pole CO_2 time series, to regional and global climate indices, and to a short record of $^{13}C/^{12}C$ isotopic ratios ($\delta^{13}C$) in atmospheric CO_2. The adaptive and evolutive nature of SSA allows us to characterize the temporal variations in CO_2 and relations between CO_2 and selected climate indices in more detail than has been reported previously. This characterization shows that, beneath the strong trend in the CO_2 series, there are relatively clear indications of interannual terrestrial and oceanic influences on CO_2 concentrations.

The datasets and SSA methodology used in the present analysis are described in the next section. The third section reports on organized modes of CO_2 variation found by SSA in the Mauna Loa and South Pole series and then compares the gradual increases in the seasonal CO_2 cycle, and interannual CO_2 variations, with global and regional temperatures. The fourth section presents joint analyses of pairs of these time series to identify coherent variations shared by CO_2 and regional climate indices, and by CO_2 and $\delta^{13}C$. A final section discusses our findings.

2. Data and methods

Since March 1958, atmospheric CO_2 concentrations have been monitored almost continuously by the Scripps Institution of Oceanography's Continuous Monitoring Program at Mauna Loa Observatory on the island of Hawaii (Keeling et al., 1976, 1982; Keeling and Whorf, 1994). CO_2 concentrations have also been monitored at the South Pole (Keeling and Whorf, 1994), episodically since 1957 and more-or-less continuously since about 1965. These two sites have been complemented by many other CO_2 monitoring stations around the world in more recent years (WMO, 1984), but the Mauna Loa and South Pole records provide the only continuous instrumental series of CO_2 concentrations that are long enough and regular enough for the present purposes.

Monthly mean mole fractions of CO_2 in water-vapor free air at Mauna Loa and the South Pole are available starting from about 1957, based on daily averages of nearly continuous observations from an infrared gas analyzer at Mauna Loa (Bacastow et al., 1985) and (mostly) on biweekly air samples from the South Pole (Keeling and Whorf, 1994). During the 442-month period of Mauna Loa record used here, from March 1958 through December 1994, 5 months of data are missing and were replaced by interpolation using a spline fit to the remaining data (Press et al., 1989). Bacastow et al. (1985) reviewed sources of error and drift in the CO_2 series, describing daily measured variances of no more than about 0.3 $(\mu mol/mol)^2$ and thus standard deviations of the monthly averages that are only about 0.1 μmol/mol. Errors in the data associated with long-term instrumental drifts and biases are larger, but should influence only the trend components in the present analysis. The monthly Mauna Loa CO_2 series analyzed here is from the Oak Ridge National Laboratory's Carbon Dioxide Information Analysis Center (CDIAC) Numeric Data Product NDP001R3.

The South Pole CO_2 record is less complete and has larger potential errors in its estimates of monthly means. The more-or-less continuous part of the South Pole record begins in February 1965; of the 341 months between then and June 1993, 26 months of data were missing and were replaced by a spline fit to the remaining data. The monthly South Pole series used here is from CDIAC's

Trends '93 data set (Keeling and Whorf, 1994). Mostly on the basis of the allowed differences between replicates in biweekly samples of 0.4 μmol/mol, the potential range of errors in the estimated monthly means at the South Pole is presumably larger than at Mauna Loa. Consequently, we focus on the more complete and accurate Mauna Loa record, but the South Pole record and discussion of shorter records elsewhere provide useful comparisons.

CO_2 concentrations are analyzed here by SSA, a form of principal-component analysis applied in the lag-time domain (Colebrook, 1978; Broomhead and King, 1986; Fraedrich, 1986; Vautard and Ghil, 1989; Vautard et al., 1992), following the implementation of Dettinger et al. (1995b). SSA generates orthonormal, data-adaptive filters that are derived from the eigenvector basis of the time series' lag-correlation matrix. By projecting it onto this basis, SSA decomposes a time series into oscillatory, trend, and noise components that are uncorrelated at zero lag. A recent expository review can be found in Ghil and Yiou (1996).

In the present application of SSA, the strong trend in atmospheric CO_2 since 1958 will be isolated, followed by the strong seasonal cycle; this permits the detection and detailed description of the much weaker interannual modes. SSA can also be used to reconstruct selected principal components so that narrow frequency bands detected by SSA can be analyzed in isolation from the remainder. This property of SSA is used here to reconstruct seasonal and interannual CO_2 variations, including slow changes in their amplitudes and phases.

A bivariate version of SSA is also used to identify oscillatory modes that CO_2 concentrations share with selected regional climatic series. Multivariate SSA (M-SSA) is a direct extension of the univariate form of SSA to include variations in several series simultaneously (Vautard et al., 1992; Jiang et al., 1995; Ghil and Yiou, 1996, and further references there). M-SSA decomposes vector-valued time series by data-adaptive filters derived now from eigenvectors of a matrix of the series' auto- and cross-lag correlations. As in univariate SSA, leading principal components of the series typically constitute trends, oscillatory modes, or noise. M-SSA modes may capture more or less of the variance of each scalar time series included in the analysis; when an oscillation is strong in more than one series, a relatively stationary phase relation between the two or more series involved is implied (for the particular oscillation captured by that mode). This capacity for detecting phase relations and their change in time motivates our use of M-SSA.

In the present analysis, a two-variable SSA was applied to CO_2 concentrations and various climatic series in order to identify climate signals that share the interannual modes observed in atmospheric CO_2. Results from SSA and M-SSA analyses with a window width — i.e., maximum lag retained — of $M = 6$ years are shown in this paper; varying the window widths between 5 and 8 years did not change the major results. Variations with periods greater than the SSA window width are lumped into trend components when SSA is applied judiciously. They were removed here by a separate prefiltering in the first steps of the analyses, using methods that are described in the next section. Variations with periods longer than one year and shorter than this 6-year cutoff constitute the interannual variations investigated here.

Relations between tropical, hemispheric, and continental climate indices, on the one hand, and CO_2 concentrations, on the other, were studied by M-SSA of (a) CO_2 together with a series of monthly average sea-surface temperatures (SSTs) in the tropics (between 20°S and 20°N latitude), globally and for each ocean basin (Parker et al., 1995); (b) CO_2 together with monthly average NH land surface-air temperature anomalies (Jones et al., 1986c; CDIAC Product NDP003R1); and (c) CO_2 together with average Palmer hydrologic drought indices from climate divisions in the north-central United States [using NOAA Climatic Data Center (NCDC) records]. Findings from these joint analyses are confirmed or extended by similar analyses (not generally shown here) with other climate indices, including Niño-3 SSTs (SSTs averaged over the so-called Niño-3 region of the tropical Pacific, i.e., between 5°S and 5°N and 150°W and 90°W; Jiang et al., 1995) and the Southern Oscillation Index (SOI; e.g., Keppenne and Ghil, 1992). Global gridded time series of SSTs (Parker et al., 1995) and land air temperature anomalies (Jones et al., 1986a; CDIAC Product NDP020) were band-pass filtered (Kaylor, 1977) and analyzed by simple statistics,

including correlation with selected CO_2 modes, in order to map regions that vary along with the CO_2 concentrations. Raw and filtered divisional Palmer hydrologic drought indices for the climatic divisions of the contiguous United States were analyzed by correlation with corresponding divisional temperatures and precipitation.

Finally, to test our interpretations regarding the relative roles of changes in marine upwelling and terrestrial ecosystems in establishing the interannual CO_2 variations identified in both the Mauna Loa and South Pole series, an 11-year series of monthly ^{13}C isotopic ratios of atmospheric CO_2 was analyzed jointly with the corresponding time interval in the Mauna Loa CO_2 concentration series. Terrestrial and marine sources of CO_2 have different $^{13}C/^{12}C$ ratios so that analysis of $\delta^{13}C$ series is used to differentiate between sources of atmospheric CO_2. The $\delta^{13}C$ series spans the interval 1978–88 and had already been "seasonally adjusted" by Keeling et al. (1989, Table B.1) by fitting a stiff "spline in tension" to Mauna Loa and South Pole $\delta^{13}C$ series and then averaging the results from the two sites. Because the series is short and prepared differently from the others in this study, its properties are less certain. Still, the joint SSA of $\delta^{13}C$ and Mauna Loa CO_2 was a valuable check on our previous results.

3. Trends and periodic CO_2 variations

3.1. Prefiltering the CO_2 series

Unfiltered monthly averages of CO_2 concentrations at Mauna Loa are shown as the light curve in Fig. 1a. The well-known trend toward increased concentrations is evident, and applying SSA to the *raw* CO_2 series shows that the trend constitutes 97.6% of its variance. To allow a better characterization of changes in the seasonal cycle and interannual variations, the raw series was detrended prior to our main SSA application using the pair of trend filters of Robertson (1996). This procedure is a simple variation on using the leading pair of (symmetric and antisymmetric) SSA eigenvectors for detrending (Ghil and Vautard, 1991). Instead of using the SSA method, we applied a simple uniformly weighted moving-average filter, followed by a linearly weighted moving-gradient filter, to remove the longest periods and periods closer to (but still longer than) the SSA window length, respectively. In the present analysis, because of the strong and nearly monotonic trend in the CO_2 series, these idealized filters yield results similar to those obtained by the usual SSA detrending (Dettinger et al., 1995b). The idealized filters were used to avoid possible removal of higher-frequency components, along with the trends removed; this also should help avoid artificial flattening of the trend components being removed near the ends of the series (Allen, 1992). An SSA window width of $M = 72$ months (i.e., 6 years) is used in the analyses presented here. Experimentation with window widths from 5 to 8 years (not shown) indicated that the results are not sensitive to the specific choice of this analysis parameter.

The raw Mauna Loa series also includes a strong seasonal cycle, which contributes 2.2% of the series' variance. The long-term (1958–94) average monthly concentrations, in a version of the series that was detrended as discussed above, form a seasonal cycle that has a peak-to-trough amplitude of about 6 μmol/mol, with maximum concentration in May and minimum concentrations in September–October (heavy curve in Fig. 1b). Notice that the times of maximum CO_2 change are likely to be associated with times of maximum net source or sink activity. The maxima and minima in Fig. 1b (and in Fig. 2b below) occur when the net balance between sources and sinks is reversing and not when the net source or sink is largest. The boreal winter increases in CO_2 concentrations have been attributed — using $\delta^{13}C$ isotopic models (e.g., Keeling et al., 1989; Ciais et al., 1995) — to the net excess of CO_2 release into the atmosphere by terrestrial respiration over CO_2 absorption by the oceans during the season when the world's larger land masses are experiencing reduced light and colder temperatures. The boreal summer decreases reflect the NH landmasses' warm-season photosynthetic uptake of CO_2 and reduced marine solubility. When this mean seasonal cycle is subtracted from the Mauna Loa CO_2 series, the heavy curve in Fig. 1a results. Notice that, once the mean seasonal cycle is removed, the trend in CO_2 concentrations is not strictly monotonic, but instead is interrupted by abrupt drops (e.g., 1973) and longer flat steps (e.g., 1990–93).

Although the same long-term CO_2 trend is evident in the raw South Pole series (Fig. 2a), the

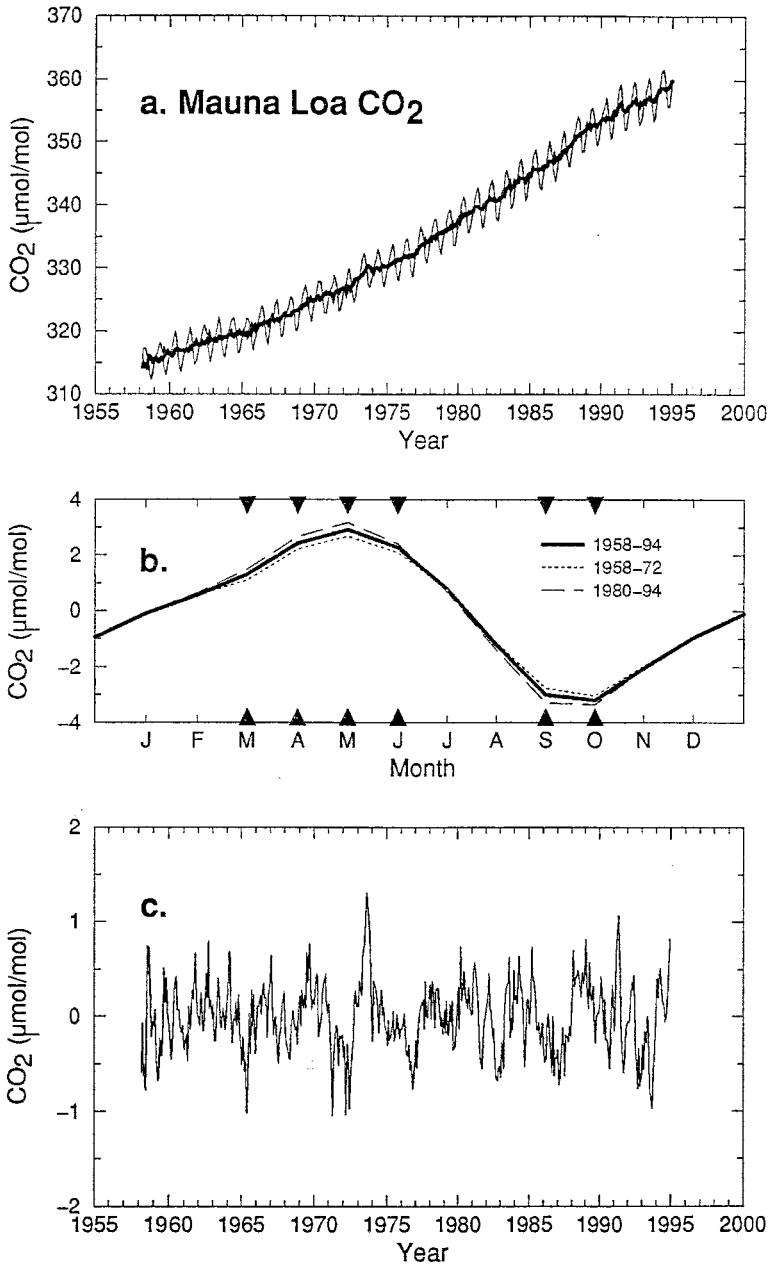

Fig. 1. Variations in CO_2 concentrations (μmol/mol) at Mauna Loa, Hawaii, as (a) unfiltered mean-monthly concentrations (light solid) and concentrations with monthly-mean seasonal cycle subtracted (heavy solid); (b) monthly-mean seasonal CO_2 cycle (January–December) from all years of record of detrended CO_2 series (solid), as well as from first part (dotted), and last part (dashed) of record; and (c) detrended CO_2 concentrations with monthly-mean seasonal cycle for the entire record removed. Solid arrowheads in panel (b) indicate months in which the 1958–72 and 1980–94 means are significantly different from each other, according to a Student-*t* test, with confidence levels greater than 95%. Monthly-mean seasonal cycles are computed from monthly means after the series was detrended by Robertson's (1996) method.

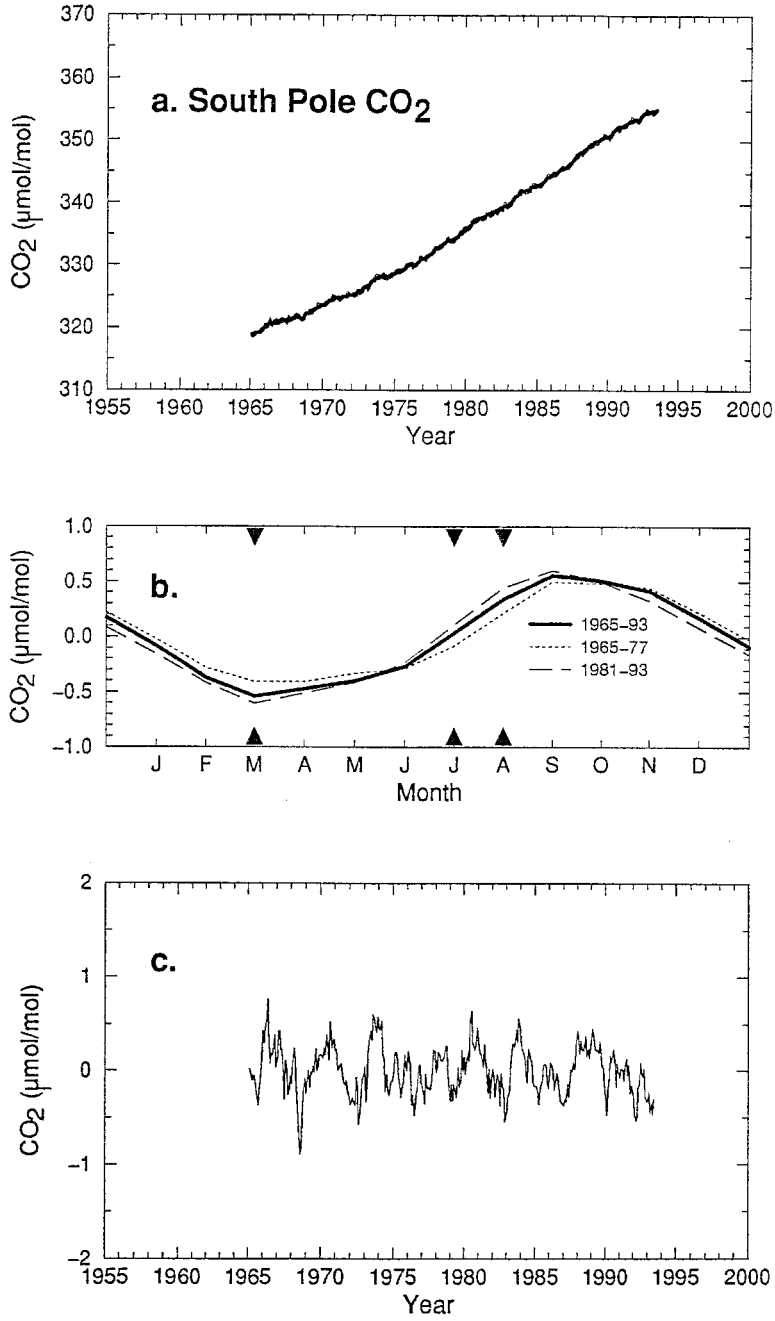

Fig. 2. Same as Fig. 1, except for variations of CO_2 concentrations at the South Pole. Raw data in Fig. 2a are difficult to discern from the deseasonalized series. Arrowheads in panel (b) indicate months in which differences between 1965–77 and 1981–93 means are significantly different from each other at the 90% confidence level.

seasonal cycle is much smaller than at Mauna Loa. The seasonal CO_2 cycle at the South Pole is so small that the raw series (light curve) in Fig. 2a is lost in the thick "deseasonalized" curve. The long-term mean seasonal cycle at the South Pole (Fig. 2b) is out of phase with the Mauna Loa cycle, reflecting Southern Hemisphere seasons. Although not shown here, CO_2 records from Point Barrow in northern Alaska (Keeling and Whorf, 1994) and Alert Station near northwest Greenland (Conway et al., 1994) also have seasonal cycles that are very different from those at Mauna Loa or the South Pole; the Arctic seasonal cycles are much larger than at Mauna Loa and also are shaped differently, with an asymmetric form dominated by a brief, deep CO_2 minimum in September and October that reflects the brief surge of photosynthesis during the short Arctic summers (Ciais et al., 1995). Thus, seasonal CO_2 cycles vary significantly from place to place in response to local uptake and release of CO_2 at the surface of land and oceans.

The seasonal CO_2 cycles at both Mauna Loa and the South Pole have changed with time. For example, it is apparent in Fig. 1a that removal of the long-term average seasonal cycle does not remove all the seasonal variations from the Mauna Loa series. Notice that the heavy, deseasonalized curve in Fig. 1a shows little seasonal variation in the early years of the record, but, by the 1990s, has clear annual residuals that are in phase with the mean seasonal cycle and almost one-third as large as it. Thus, the seasonal cycle of CO_2 concentrations, as noted already by Bacastow et al. (1985), has increased in recent decades well beyond its long-term average amplitude.

The 15-year-mean seasonal cycles from the beginning and end of a detrended version of the Mauna Loa CO_2 series are shown as dotted and dashed curves in Fig. 1b. Comparison of the three curves in Fig. 1b indicates that the average change in the seasonal CO_2 cycle, from the beginning to the end of the Mauna Loa record, occurred mainly as an increase by $+1$ μmol/mol in the cycle's peak-to-trough range. The nearly symmetric timing of the largest changes, positive and negative, in Fig. 1b is largely an artifact of the detrending, so it is difficult to decide during which seasons CO_2 has increased or decreased most, except in relative terms. The shape of the seasonal cycle has changed slightly, however, and this is not a function of detrending. Although the shift is difficult to discern in these monthly data, mean March and mean September concentrations seem to have increased and decreased, respectively, so as to hasten the arrival of the spring maximum and autumn minimum of CO_2. Thus, along with an increase in amplitude, the phase of the seasonal CO_2 cycle has shifted towards earlier in the year in recent decades. Similar shifts towards an earlier seasonal cycle are more obvious at the South Pole (Fig. 2b) where the shift is imposed on a smaller overall cycle and at Point Barrow (not shown) where it is imposed on a very asymmetric cycle.

The detrended Mauna Loa series retains a large seasonal cycle that limits the interpretation of the faint interannual signals. The analysis of interannual variations was based, therefore, on a detrended and deseasonalized version of the CO_2 series (Figs. 1c, 2c). These series were obtained by detrending the "deseasonalized" heavy curves in Figs. 1a, 2a. Significant subannual, seasonal, and interannual variability remain in these series, although the magnitude of these variations is but a small fraction of the raw CO_2 variability.

3.2. *Long-term variations of the seasonal CO_2 cycle*

The depiction of the changing seasonal cycles using the series in Figs. 1c and 2c is complicated by a resulting characterization of smaller-than-average seasonal cycles during the time interval centered on the 1970s as having negative amplitudes. To simplify visualization, therefore, we performed a separate SSA on detrended but not deseasonalized CO_2 series (which does not yield negative amplitudes) for the discussions in this section, whereas in the remainder of this paper, CO_2 variations will be discussed in terms of the SSA of the detrended *and* deseasonalized series (Figs. 1c, 2c).

Variations of the seasonal CO_2 cycle's amplitude were characterized by SSA of the detrended but not deseasonalized CO_2 series, with a window width of 72 months. The SSA results for the detrended Mauna Loa series are dominated by the mean seasonal cycle and its long-term variations. The boreal-winter variations are illustrated in Fig. 3a; the envelope of boreal-summer variations (not shown) is virtually the negative of the envelope shown. The time-varying amplitude (heavy curve, Fig. 3a) and changes in phase

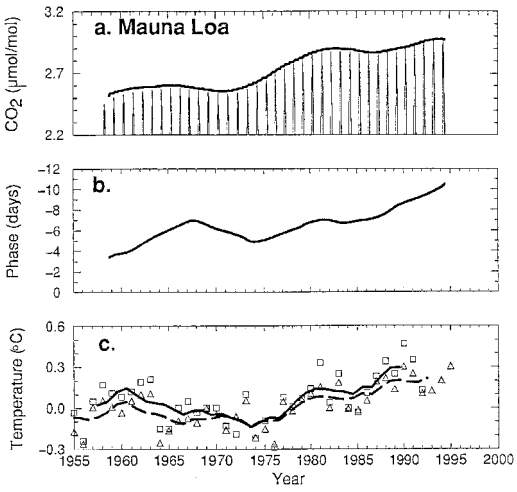

Fig. 3. (a) Long-term variations of Mauna Loa seasonal CO_2 cycle, from singular-spectrum analysis (SSA) of detrended CO_2 series, as sum of reconstructed SSA components 1 and 2 (light curve) and amplitude envelope by method of Plaut and Vautard (1994) (heavy curve); (b) annual-mean phase of Mauna Loa seasonal CO_2 cycle by method of Plaut and Vautard (1994); and (c) Northern Hemisphere (NH) mean temperature anomalies (squares and solid curve) and global-mean temperature anomalies (triangles and dashed curve). Only the positive upper part of the variations is shown in (a) but the negative part is essentially symmetric. Curves in (c) are 6-year moving averages; temperature anomalies are deviations from the 1951–70 means.

(Fig. 3b) of the seasonal CO_2 cycle were determined by annually averaging the direction and amplitude, in the complex plane, of a complex-valued time series with real part equal to the SSA reconstruction (light curve, Fig. 3a) and imaginary part equal to its time rate of change (see Plaut and Vautard, 1994, and Moron et al., in press, for other uses of this decomposition). The Mauna Loa seasonal CO_2 cycle is characterized by relatively stable amplitudes in the 1960s, a decrease to minimum amplitudes around 1970, a rapid increase through the 1970s, another slight minimum around 1987, and then renewed increases until at least 1994. The phase of the seasonal CO_2 cycle has shifted towards progressively earlier occurrence of the seasons, totalling about 8 days between 1958 and 1995, with local maxima in 1968 and 1981.

The sequence of changes in the amplitude of the seasonal CO_2 cycle at Mauna Loa nearly parallels the progression of global and NH mean temperatures in recent decades (Fig. 3c). Correlations of the amplitudes and phases of the Mauna Loa (and South Pole) seasonal CO_2 cycles with long-term global and hemispheric surface-air temperature trends are listed in Table 1. Variations of the amplitude of the seasonal CO_2 cycle at Mauna Loa correlate well with global-mean temperatures and NH-land temperatures, but less well with overall NH-mean temperatures. The amplitude of the seasonal CO_2 cycle is about equally correlated with NH summer and winter temperatures, but the correlation coefficient for those two temperature series is also 0.90 (giving a confidence level greater than 95%).

The parallel between global temperatures and the amplitude of the seasonal cycle of CO_2 concentrations has been noted by Keeling et al. (1996), using other time-series analysis methods based on fitted harmonics and splines in tension (Keeling et al., 1989). They have suggested that the recent warmer climate has fostered vegetation growth and attendant increases in photosynthesis, and decreases in CO_2, during the warm seasons and increased respiration, with increases in CO_2, during the cool nongrowing seasons. Nemry et al. (1996) used a mechanistic vegetation model to show that, in most of the NH, temperate ecosystems dominate the seasonal CO_2 cycle but, near the latitude of Mauna Loa (21°N), tropical ecosystems could dominate. For the slow variations of seasonality shown in Fig. 3, the various hemispheric temperatures all share much the same trend and the source of seasonal-cycle changes can not be distinguished by correlations alone. The CO_2 seasonality trends also are broadly similar to recent global land-precipitation trends (Keeling et al., 1995), although Knorr and Heimann (1995) argue that water availability has little impact on the seasonal CO_2 cycle. Despite these uncertainties, SSA provides a particularly clear picture of the history of the CO_2 variations for use in more detailed interpretations.

The changing phase of the seasonal CO_2 cycle at Mauna Loa may be associated with changing temperature seasons over the NH land masses. Table 1 indicates that the changing phase of the seasonal CO_2 cycle at Mauna Loa is only modestly correlated with the global and hemispheric temperature trends (given the few degrees of freedom in these smoothed series). Although the seasonal

Table 1. *Correlations between amplitude, A(t), and phase, $\phi(t)$, of CO_2 seasonal cycles and 6-year moving averages of hemispheric and global temperature series*

		Temperatures					
CO_2 record	Amplitude and phase	Global mean	NH mean	NH-land mean	SH mean	May–Oct. mean	Nov.–Apr. mean
Mauna Loa	$A(t)$	**+0.81**	+0.66	**+0.81**	**+0.81**	+0.78	+0.76
(1959–1993)	$\phi(t)$	−0.67	−0.46	−0.69	**−0.81**	−0.71	−0.58
South Pole	$A(t)$	+0.67	+0.57	+0.70	+0.74	+0.66	+0.65
(1966–1922)	$\phi(t)$	**−0.92**	+0.88	−0.84	**−0.94**	**−0.92**	−0.89

Correlations that are significantly different from zero at 95% confidence levels (for Mauna Loa) and 90% levels (for the South Pole) are in boldface. May–October and November–April means are means of Northern Hemisphere (NH) temperatures for Mauna Loa and Southern Hemisphere (SH) temperatures for the South Pole.

cycle of surface-air temperatures has also varied in recent decades (Kuo et al., 1990; Thomson, 1995; Mann and Park, 1996), the CO_2 phase shift (totalling about 7 days) is much larger than the phase shifts found in the seasonal cycle of global temperatures (no more than a single day over the course of this century). While the reasons for the small changes in the global seasonal cycle of temperatures are far from settled (Karl et al., 1996; White et al., 1996; Thomson, 1996), the seasonal-cycle variations of Mauna Loa CO_2 and NH-land surface-air temperatures (1958–95) are in part coherent, as will be found in Subsection 4.3 by an application of bivariate SSA to the series. Also, the phase shifts in Mauna Loa CO_2 are similar to observed 5- to 15-day shifts in the seasonal cycles of surface-air temperatures over the NH land masses (Mann and Park, 1996).

The corresponding sequences of changes in the amplitude and phase of the seasonal CO_2 cycle at the South Pole are shown in Figs. 4a, b. The amplitude changes appear to differ from the changes at Mauna Loa in timing as well as magnitude. The changes in the amplitude of the seasonal cycle at the South Pole do not appear to follow Southern Hemisphere (SH) mean land air temperatures on annual or seasonal time scales (Table 1 and Fig. 4c) or the global mean temperatures (Fig. 3c). The phase shift, however, does mirror the trend of SH mean temperatures. A larger phase shift (Fig. 4b) is indicated at the South Pole (18 days earlier over 27 years) than at Mauna Loa (7 days over 38 years). The tendency for the amplitude of the Mauna Loa seasonal CO_2 cycle to follow hemispheric temperatures, whereas it is the phase of the South Pole seasonal CO_2 cycle that follows them, may provide clues to the origin of the observed seasonality changes.

To identify areas with the largest changes in temperature seasonality, standard deviations of narrowly band-pass filtered temperature anomalies from two sources were mapped. Long-term monthly mean temperatures were subtracted, at each grid point, from 5°-latitude × 5°-longitude

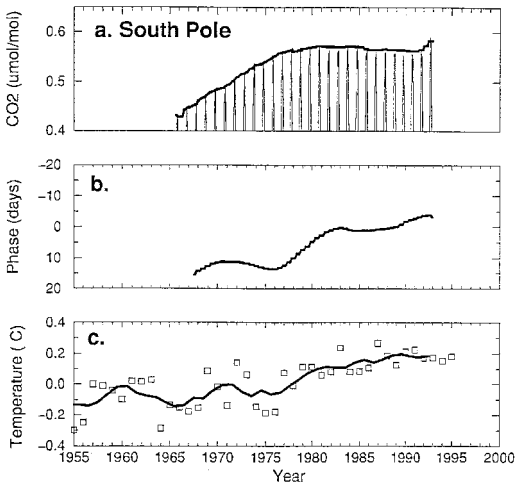

Fig. 4. (a) Long-term variations of South Pole seasonal CO_2 cycle, as in Fig. 3, from SSA of detrended CO_2 series (only upper part of the variations is shown but lower part is nearly symmetric); (b) annual-mean phase of the South Pole seasonal CO_2 cycle by method of Plaut and Vautard (1994); and (c) SH mean temperature anomalies (squares and solid curve). Curve in (c) is a 6-year moving average; temperature anomalies are deviations from 1951–70 means.

gridded global surface-air temperatures based on the longest instrumental temperature series available (Jones et al., 1986a, 1986b). The resulting temperature anomalies were narrowly band-pass filtered (Kaylor, 1977) with half-power points at 11 and 13 months to separate remaining variations from the long-term seasonal cycle. Standard deviations of these 12-month temperature variations are shown as shades of gray in Fig. 5. The regions that have experienced the largest changes in temperature seasonality are the northern land masses (also see Myneni et al., 1997). Not surprisingly, SSTs (especially in the Tropics) have experienced only small seasonality changes.

A similar spatial pattern of standard deviations is found in the shorter, but more accurate, Microwave Satellite Unit (MSU) record of lower tropospheric air temperatures (contoured in Fig. 5). Correlations (not shown) between Mauna Loa CO_2 and the narrowly filtered surface-air temperature anomalies indicate that the temperature variability mapped in Fig. 5 is essentially in phase with Mauna Loa CO_2 seasonality on the extratropical continents, especially over North America, and apparently out-of-phase over most of the tropical continents (although the signal is very weak in the tropics). Changes in both the amplitude and phase of the seasonal cycles of CO_2 concentrations and surface-air temperatures (Mann and Park, 1996) contribute to the anomalies analyzed so far. Further light will be shed on the matter by the bivariate SSA in Section 4.3.

3.3. *Interannual CO_2 variations*

After detrending with Robertson's (1996) filter pair (see Section 3.1), the mean seasonal CO_2 variation at Mauna Loa, peak-to-trough, is about 6 μmol/mol (see Fig. 1b and discussion thereof); variations of CO_2 concentrations ranging over about ± 1 μmol/mol remain after this mean cycle is removed. These interannual CO_2 variations are characterized best by SSA of the detrended and deseasonalized series in Figs. 1c, 2c, for Mauna Loa and the South Pole, respectively. SSA captures oscillatory modes within a time series in the form of pairs of orthogonal components that express nearly equal fractions of the variance of the time series and that have temporal manifestations — empirical orthogonal functions and principal components — that are in quadrature with

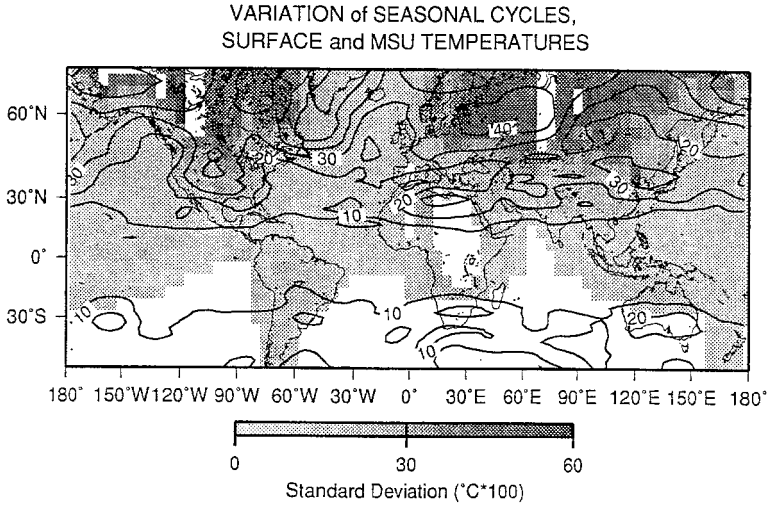

Fig. 5. Standard deviations of monthly anomalies from long-term mean seasonal cycles of temperature, band-pass filtered with half-power points at 11 and 13 months. The sea-surface and land surface-air temperature results for 1958–95 are shaded, and the results for Microwave Sounding Unit (MSU) satellite channel-6(2R) measurements of lower tropospheric temperatures are contoured. MSU temperature estimates for 1979–95 are centered near 750 hPa with half-weighting points near 400 and 1000 hPa (Spencer and Christie, 1992). Only grid points with at least 30 years of continuous recent surface observations (for estimation of long-term mean seasonal cycles) are shaded.

each other (Vautard and Ghil, 1989; Dettinger et al., 1995b).

In the present SSAs, we address CO_2 variations that are probably not reflections of simple dynamical oscillations but rather reflect many concurrent processes. Thus, in analyzing these variations, our focus is on the characterization of concentrated, but broad-peak, variance rather than single, pure sine waves. In this analysis, therefore, significance tests that compare SSA components to ideal sine waves (Allen and Smith, 1996) are probably not suitable. Instead, we used simple considerations to focus analysis on the most powerful components. Later, these components are shown to be related to SST oscillations with frequencies like tropical-temperature modes that have been found to be highly significant relative to the most rigorous statistical tests (Allen and Smith, 1996; Mann and Park, 1996).

Using the same 72-month window as before, SSA of the detrended and deseasonalized CO_2 series produced three pairs of SSA modes (components 1–2, 3–4, and 5–6) that stand out above the noise floor of an eigenvalue scree plot (Fig. 6a) and that are thus regarded as consequential (Vautard et al., 1992). The pairs 1–2 and 5–6 together capture about 38% of the variance in the Mauna Loa series, after detrending and deseasonalizing. The variations captured have spectral peaks (Fig. 6b) at roughly 4 years (especially apparent in the first pair) and 3.1 years (enhanced in the third pair). The pair 3–4 captures the 13% of variance due to the seasonal-cycle variations that were discussed in Subsection 3.2.

The sum of the reconstructed components (RCs: Ghil and Vautard, 1991; Dettinger et al., 1995b) associated with the interannual CO_2 variability is shown in Fig. 7a for Mauna Loa and in Fig. 7b for the South Pole. El Niño years — such as 1977, 1983, 1987, and the early 1990s — have a substantial effect on the interannual variability of Mauna Loa CO_2 concentrations. The remarkable string of El Niño/La Niña years between 1970 and 1977 is also notable as the time interval of extreme interannual CO_2 fluctuation in both records: 1970, 1973, and 1977 were El Niño warm events, whereas 1971, 1974, and 1976 were La Niña cool events. The 1983 El Niño did not elicit an unusually large CO_2 response in either the raw or SSA-reconstructed series at either location (see also Meyers and O'Brien, 1995) and is not an unusually large

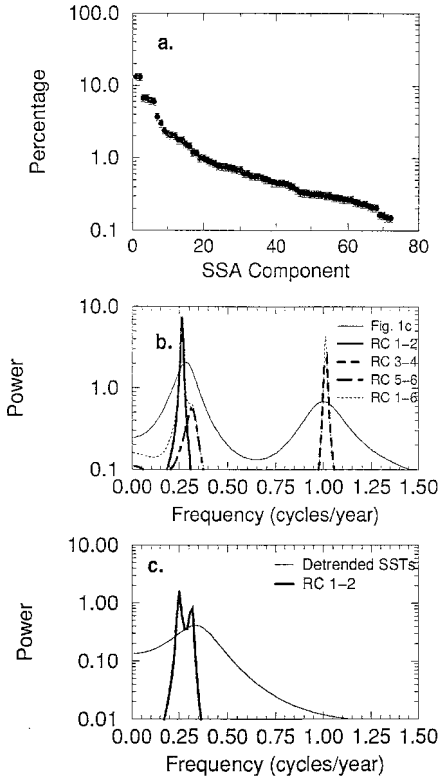

Fig. 6. (a) SSA eigenvalue spectrum as percentage of variance captured by each SSA component of the detrended, deseasonalized Mauna Loa CO_2 series in Fig. 1c; (b) maximum-entropy stack spectra for raw and leading reconstructed SSA components (RCs); and (c) maximum-entropy spectra for detrended tropical SSTs and their leading RCs. Error bars in panel (a) are $\delta\lambda_k = (2\tau/N)^{1/2}\lambda_k$, where τ is a typical decorrelation time (assumed here, very conservatively, to be 2 years, whereas the observed e-folding time is several months), N is the number of observations (442 months), and λ_k is the kth SSA eigenvalue (Dettinger et al., 1995a, eq. (5)).

excursion in the (oscillatory) SSA-reconstruction of the tropical-belt SSTs; that extreme event falls outside the regular, oscillatory variations of the tropical SSTs captured by the leading SST components.

El Niño episodes involve reduced upwelling of deep, cool, CO_2-rich sea waters in the Equatorial Pacific (Murray et al., 1994; Meyers and O'Brien, 1995), and the beginning of El Niño episodes often is accompanied by a marked interval of reduced atmospheric CO_2 concentrations, associated with the interruptions in upwelling and CO_2 outgassing

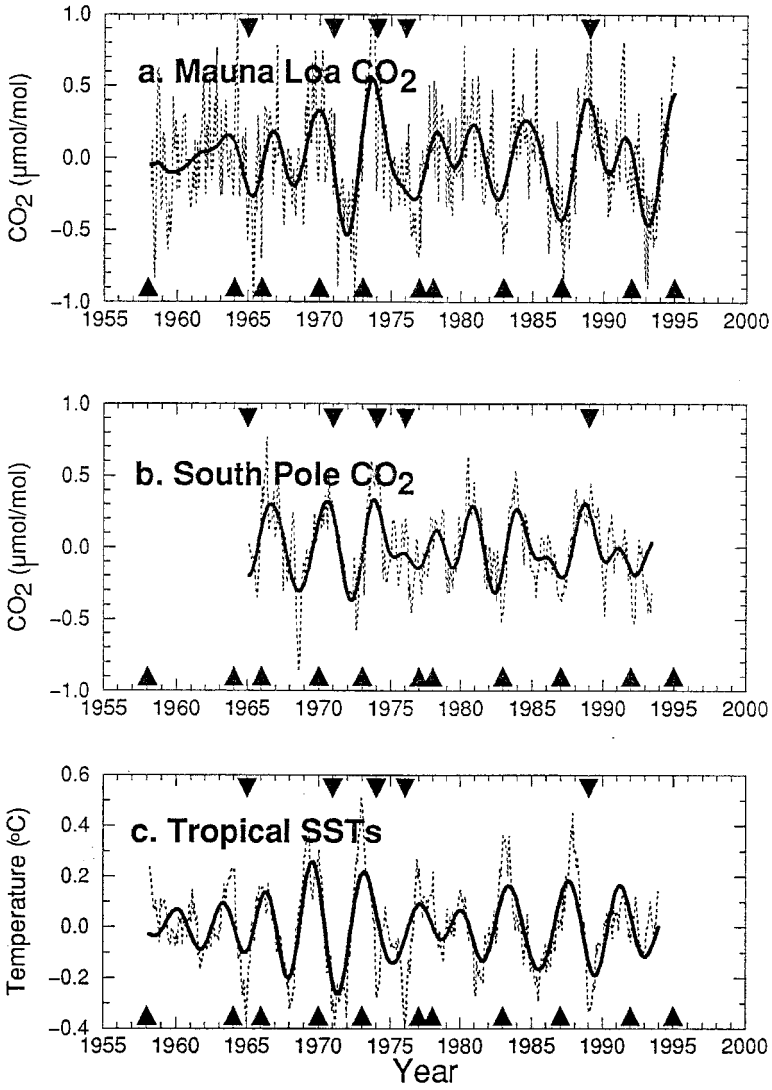

Fig. 7. (a) Interannual CO_2 variations obtained from SSA of the detrended, deseasonalized Mauna Loa series in Fig. 1c; (b) same as panel (a) for the South Pole series in Fig. 2c; and (c) mean-monthly sea-surface temperature (SST) anomalies between 20°S and 20°N. In each panel, the sum of leading RCs is shown by heavy solid lines and the "raw" signal by light dotted lines. Upward-pointing arrowheads indicate January 1 of mature phase El Niños; downward-pointing arrowheads indicate La Niñas.

(Figs. 1a, 2a, 7a; Meyers and O'Brien, 1995). Strong rebounds in CO_2 concentrations soon after the warm events have begun are also evident in Fig. 7a and even in Fig. 1c. El Niños also result in significant regional and, ultimately, global increases in air temperature (Angell, 1990; Ghil and Vautard, 1991). Presumably, much of the positive rebound of CO_2 during the warm episodes in the tropical Pacific is due to the indirect effects of global temperature and precipitation changes associated with these episodes on the terrestrial biosphere, which yield net sources of CO_2 that more than compensate for decreases in CO_2 outgassing from the tropical oceans (see Section 1

and Keeling et al., 1989; Siegenthaler, 1990). La Niñas followed by El Niños in rapid succession contribute some of the appearance of CO_2 declines at the beginning of El Niños. Finally, both the initial CO_2 decline and the eventual resurgence may reflect the overall lag between SST and CO_2 variations (discussed in greater detail later). The Mauna Loa interannual variations in Fig. 7a are shared with the South Pole CO_2 series, as indicated by the close correspondence between the interannual components extracted from the two series by separate univariate SSA (Fig. 7b) as well as by a bivariate SSA of the two series (not shown).

Interannual variations of the mean SSTs in the global tropics between 20°S and 20°N (isolated by SSA with the same window size) are shown in Fig. 7c. The warming influence of El Niño events is clear in this series and the filtered variations bear a remarkable similarity to the corresponding interannual CO_2 variations in Figs. 7a, b. The SST spectra (Fig. 6c) confirm that the same two interannual periodicities, of about 3 and 4 years, are captured in CO_2 and SST, although they are lumped into a single SSA pair (1–2) in the SSTs. The large variability of the seasonal cycle (pair 3–4 in Mauna Loa CO_2) is not a leading component of the tropical-belt SSTs. Although the phase relations are not constant, the interannual Mauna Loa CO_2 and tropical SST variations have a maximum correlation coefficient of 0.69 (which corresponds to a 94% confidence level), obtained when the CO_2 variations lag behind (i.e., occur later than) the SST variations by about 8 months. Interannual variations of the SOI and mean SSTs for the so-called Niño-3 region (5°S to 5°N, 150°W to 90°W) are more common indices for the seasonal-to-interannual variability of the tropical Pacific (Rasmusson et al., 1990; Jiang et al., 1995) and yield the same close interannual relations to CO_2 upon SSA filtering. The general coherence of Mauna Loa CO_2 with global temperatures on interannual time scales, and a lag of roughly 5 months, were also noted by Kuo et al. (1990).

The two interannual frequencies shared by Mauna Loa CO_2 and tropical SSTs arise nearly globally in the case of the QQ variations and more locally in the case of the quasi-triennial (QT) variations. For the same 1958–1993 interval used in Figs. 6, 7, tropical SSTs in each major tropical ocean basin share spectral peaks with the CO_2 record at roughly 4 years (Fig. 8). The QQ peaks

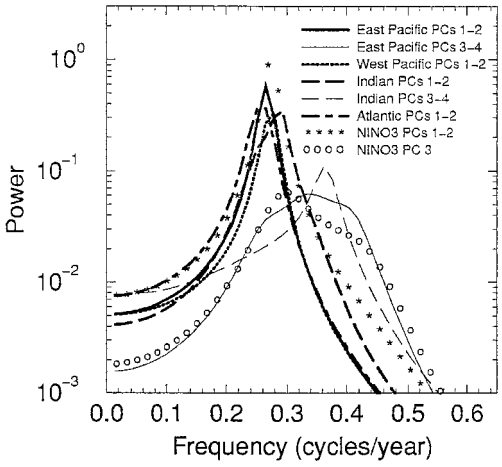

Fig. 8. Maximum-entropy spectra of leading principal components (PCs) from bivariate SSAs of detrended, deseasonalized Mauna Loa CO_2 series with tropical SSTs between 20°S and 20°N, in the eastern Pacific (150°W–80°W), western Pacific (120°E–150°W), Indian (35°E–120°E), and Atlantic (80°W–15°E) Oceans, and in the Niño-3 region of the eastern Pacific (5°S–5°N, 150°W–90°W). The analyses are all carried out over the 1958–1993 interval; see legend in figure.

are apparent in the univariate SSA of each basin's SST series (not shown) and in the bivariate SSA of each basin's SST series, in turn, with the detrended, deseasonalized Mauna Loa CO_2 (Fig. 8). A broad secondary contribution near 3 years appears principally in the eastern tropical Pacific (150°W–80°W) and possibly in the Indian Ocean in both univariate and bivariate SSAs. SST anomalies in the classical Niño-3 region confirm the secondary QT contribution, more so than the SSTs for the entire eastern tropical Pacific (cf. Fig. 8).

The eastern Pacific QT signal in SST is, in fact, stronger (when analyzed separately from CO_2) and bears a clearer relation to the CO_2 signal in the corresponding bivariate analysis than is the case for the Indian Ocean (although Fig. 8 would suggest the opposite to be the case). A cursory comparison of gridded equatorial Pacific SST anomalies with the QQ and QT modes suggests that the latter may be capturing mostly small SST excursions that enhance El Niño or La Niña episodes in the eastern Pacific, in contrast to the QQ mode which can be identified more with El Niño episodes that ultimately encompass the

entire tropical belt. The present analysis also found the well-known quasi-biennial component of tropical SSTs (Rasmusson et al., 1990; Jiang et al., 1995) among the higher-order SSA pairs of the tropical SSTs (especially in the eastern Pacific and Indian Oceans), but not among the leading CO_2 modes. A more complete spectral analysis of tropical SSTs, using longer records, is in press (Moron et al., 1997).

4. CO_2 and climate variability

To clarify and describe in greater detail phase relations between CO_2, on the one hand, and global and regional temperatures, on the other, and to more decisively distinguish between oceanic and terrestrial influences in the interannual CO_2 variations, we analyzed several pairs of detrended and deseasonalized CO_2 and climatic time series using bivariate SSA. This joint analysis is applied to extract the seasonal and interannual variations that are shared by the series in data-adaptive frequency ranges. Among the numerous analyses that we carried out, three are discussed in detail here. First, the time series shown by the light curves in Figs. 7a (Mauna Loa CO_2) and 7c (tropical-belt SST) were analyzed by two-channel SSA. Then the averages of seasonally adjusted $\delta^{13}C$ isotopic ratios from Mauna Loa and the South Pole (taken from Table B.2 of Keeling et al., 1989) were analyzed together with Mauna Loa CO_2 concentrations. Finally, the light curve in Fig. 7a (Mauna Loa CO_2) was analyzed with NH-mean land surface-air temperatures (monthly values that previously were averaged to obtain values in Fig. 3c and Table 1). The bivariate analysis of Mauna Loa CO_2 and the more local Palmer drought index for the contiguous United States are also discussed, to illustrate the joint climatic contributions of precipitation and temperature to CO_2 variations.

4.1. CO_2 and tropical SSTs

Components 1 and 2 from the joint SSA of Mauna Loa CO_2 and tropical SSTs form an oscillatory pair. In the case of M-SSA, the associated reconstructions are sequences of vectors (in the present case, 2-vectors: Vautard et al., 1992; Jiang et al., 1995; Unal and Ghil, 1995). The sum of RCs 1 and 2 isolates the QQ oscillations shown in Fig. 9a. Together these components capture 27% of the variability of the two series (see Fig. 10a) as a joint oscillation with a period of about 3.7–4 years. The sum of the spectra of the two corresponding M-SSA principal components (PC) is shown as the heavy curve in Figure 10b; the PCs from M-SSA are a univariate depiction of the shared oscillation, unlike the RCs (see Fig. 9) and like the PCs from single-channel SSA.

The bivariate oscillation captured by components 1–2 probably corresponds to the "low-frequency" (Rasmusson et al., 1990; Keppenne and Ghil, 1992; Latif et al., 1993) or QQ (Jiang et al., 1995; Robertson et al., 1995) oscillation in the tropical Indo-Pacific basin. SSTs are weighted about twice as heavily as CO_2 in the SSA components, indicating that this oscillation is stronger in the SSTs. The CO_2 and SST variations in this "low-frequency" range are approximately in phase (Fig. 9a). As would be expected from comparison of Figs. 7a–c, joint SSA of South Pole CO_2 and tropical SSTs isolates the same shared components (not shown here), also in phase, which suggests that CO_2 varies synchronously with tropical QQ variations over a very large, possibly global geographic area. Although the low-frequency tropical

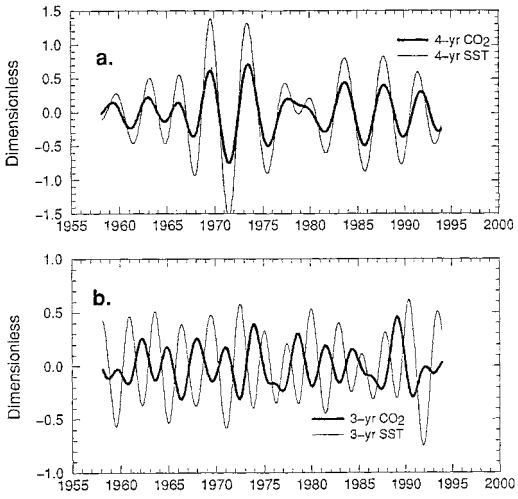

Fig. 9. Bivariate SSA reconstructions of shared interannual variability of Mauna Loa CO_2 concentrations and overall tropical-mean, SST for the (a) quasi-quadrennial (QQ) mode and (b) quasi-triennial (QT) mode. The RCs for each of the two time series (light and heavy lines) are separately identified in each panel.

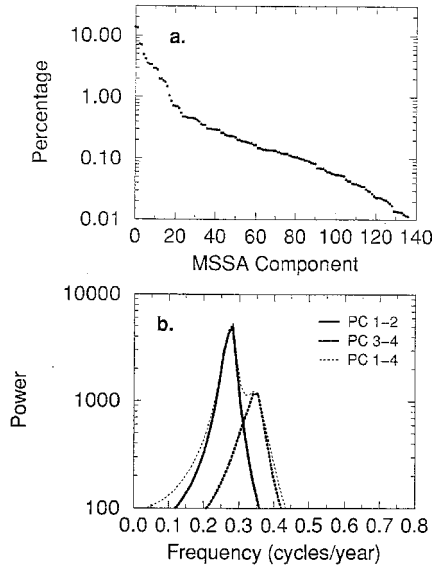

Fig. 10. (a) Bivariate SSA eigenvalue spectrum as percentage of variance captured by each M-SSA component of detrended, deseasonalized Mauna Loa CO_2 series and detrended tropical SST anomalies (in Fig. 7c) and (b) maximum-entropy spectra for leading M-SSA PCs of Mauna Loa CO_2 and tropical SSTs.

mode is reflected similarly in the Mauna Loa and South Pole CO_2 series, it may not be entirely global as the mode is difficult to identify in at least some CO_2 records elsewhere, including, for example, the 1974–88 CO_2 series from Point Barrow, Alaska (not shown here).

The QQ mode of CO_2 concentrations is thus in phase, as far as one can tell, with QQ variations of the tropical-belt SSTs. This phase relation also holds for the individual tropical basins. When area-averaged SSTs from each of the tropical basins, in turn, are analyzed by bivariate SSA with Mauna Loa CO_2, the QQ spectral peaks in Fig. 8 correspond to in-phase relations (not shown). This in-phase relation would not be expected if the reponse was due to tropical marine effects. The tropical ocean surface waters are cool when upwelling is strong; this same upwelling brings CO_2-rich water to the surface and increases the rate at which the tropical ocean releases CO_2 to the atmosphere. Increased tropical outgassing tips the balance between tropical and extratropical influences in favor of reductions or even reversals of the overall uptake of CO_2 by the oceans (Keeling et al., 1989; Ciais et al., 1995). More likely, the in-phase relation corresponds to successive phases of enhanced or diminished terrestrial ecosystem activity in response to warmer or cooler land temperatures (Angell, 1990; Ghil and Vautard, 1991) and, possibly, land precipitation variations driven by the interannual fluctuations of tropical SSTs (as discussed in the Introduction).

Components 3–4 from the same joint SSA of Mauna Loa CO_2 and tropical-belt SSTs capture 14% of the variance in both series (Fig. 10a) in the form of oscillations with periods of roughly 2.8–3 years (Fig. 10b). These components have a lower frequency than the quasi-biennial modes known from analyses of other tropospheric and oceanic fields in the tropics (Rasmusson et al., 1990; Jiang et al., 1995; Unal and Ghil, 1995) and are more likely related to the secondary, 3-year contribution in the spectrum of the tropical eastern Pacific SSTs (Fig. 8). In this QT component (Fig. 9b), CO_2 and SSTs are roughly 180° out of phase. This out-of-phase relation is also found in the corresponding modes from joint analyses of the South Pole CO_2 and tropical-belt SSTs (not shown). In the Point Barrow CO_2 series, irregular QT components were also isolated in a joint analysis with the tropical-belt SSTs; in this Point Barrow mode, CO_2 is out of phase with the tropical SSTs as well (not shown). The out-of-phase relation between these more rapid variations of tropical SSTs and CO_2 concentrations probably indicates a largely marine influence on (or interaction with) CO_2 concentrations at this time scale. Associated with the interannual fluctuations of tropical SSTs are (i) a reduction, or even reversal, of the overall ocean uptake of CO_2 when upwelling of CO_2-rich ocean waters in the tropics is strong (yielding *higher* atmospheric CO_2 concentrations), and (ii) cooler global tropical SSTs when upwelling is strong (yielding *lower* SSTs). Together, these two effects yield a negative correlation between tropical SSTs and CO_2 in response to upwelling changes.

Correlations between the reconstructed tropical-belt SST series in Figs. 9a and 9b, respectively, with gridded SSTs that have been filtered to retrieve interannual variations between 24 and 72 months are shown in Figs. 11a and 11b. The correlations depict the spatial SST patterns associated with the bivariate SSA modes of CO_2 and tropical SST. The QQ mode correlations (Fig. 11a)

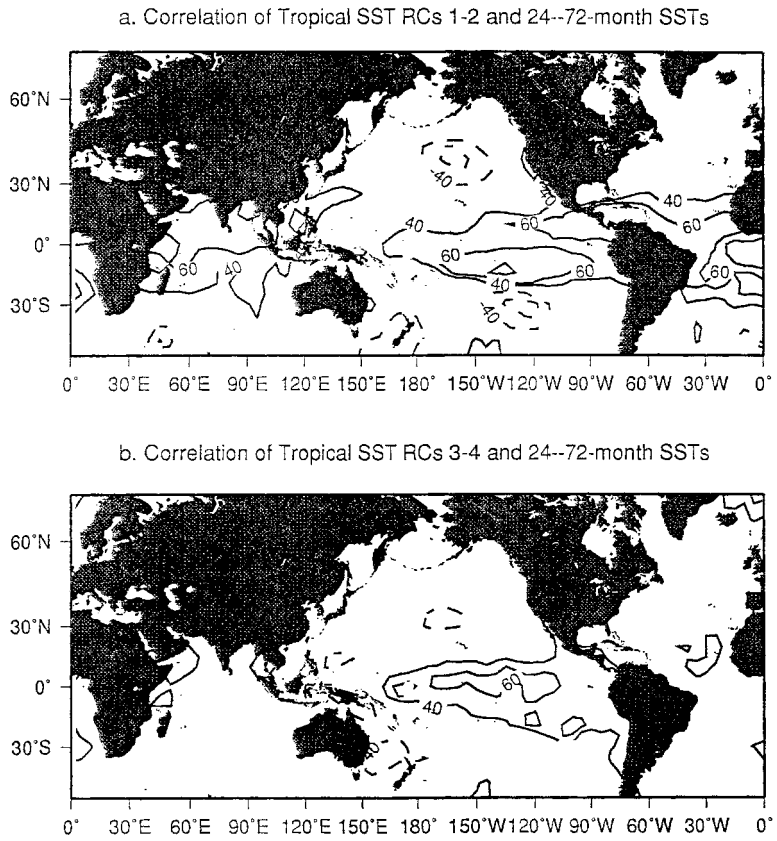

Fig. 11. Correlations between tropical-belt SST modes shared with Mauna Loa CO_2 (Fig. 9), on the one hand, and gridded global SSTs, band-pass filtered with half-power points at 24 and 72 months, on the other; (a) QQ mode (Fig. 9a) and (b) QT mode (Fig. 9b). Contours depict (dimensionless) correlations times 100, where significantly different from zero at the 90% confidence level; dashed where negative.

are strong over most of the Pacific and Indian Oceans and the tropical Atlantic, with positive correlations throughout most of the tropics. Recalling that the SST in the QQ bivariate SSA mode is in phase with Mauna Loa CO_2, the strong, widespread positive correlations in Fig. 11a indicate that near global SST warming underlies the positive QQ variations in CO_2. In contrast, the QT mode correlations (Fig. 11b) are strong almost exclusively in the tropical and subtropical eastern Pacific; elsewhere, the correlations are much weaker. Recall that the QT mode had CO_2 and tropical SST out of phase; therefore, Fig. 11b implies that atmospheric QT-scale CO_2 increases accompany mostly decreases in SST (and presumably increased upwelling) in the eastern tropical Pacific, near the Niño-3 region used routinely to monitor El Niño conditions.

Taken together, the QQ and QT components reproduce much of the (variably) lagged relation between SST and CO_2 noted in the interannual components isolated from independent (univariate) SSAs of Mauna Loa CO_2 and tropical-belt SSTs (Figs. 7a, c, respectively). Summing the RC curves of CO_2, on the one hand, and the SST curves, on the other, yields a maximum cross-correlation between the interannual variabilities (QQ and QT) of CO_2 and SST that equals $+0.65$ (i.e., provides a 92% confidence level) when the lag equals 6 months, with SST on average leading CO_2. This is quite close to the correlation of $+0.69$ (statistical significance of 94%) at 8 months

lag when the two series were filtered through separate univariate SSAs. As importantly, the variations in lags of the univariate RCs and bivariate RCs are similar over most of the 38 years of CO_2 record (except near the beginning and end where SSA reconstructions are least constrained).

4.2. CO_2 concentrations and $\delta^{13}C$ isotopic ratios

To better understand the contrast between the in-phase QQ relation of tropical SSTs and CO_2 versus the out-of-phase QT relation, the detrended and deseasonalized Mauna Loa CO_2 concentration series and a "seasonally adjusted" global $\delta^{13}C$ series for atmospheric CO_2 were analyzed together using bivariate SSA. The $\delta^{13}C$ of CO_2 in the atmosphere and oceans equilibrate with each other rapidly so that they are almost always near isotopic equilibrium on the time scales of interest here; as a consequence, at a given time, CO_2 that enters the atmosphere from the oceans has almost the same isotopic signature as the CO_2 that is already in the atmosphere. In contrast, $\delta^{13}C$ in CO_2 from terrestrial sources (including fossil fuels) is typically about -18 per mil lower (lower $^{13}C/^{12}C$ ratio) than the oceanic and atmospheric reservoirs (Keeling et al., 1989). Using this difference, measured variations of $\delta^{13}C$ in the atmosphere have been used to isolate relative contributions of marine and terrestrial CO_2 sources (Keeling et al., 1989; Ciais et al., 1995). In the present study, the joint analysis of CO_2 and $\delta^{13}C$ series thus provides a direct line of evidence for understanding the differences between QQ and QT variations in CO_2 concentrations.

The "global" $\delta^{13}C$ series used in the bivariate SSA with Mauna Loa CO_2 was obtained by averaging the seasonally adjusted $\delta^{13}C$ at Mauna Loa and the South Pole (averaging performed by Keeling et al., 1989, table B.2). A shared QQ mode was isolated by using a window length of 50 months (to accommodate the short length of the $\delta^{13}C$ record); this mode captures 29% of variance (Fig. 12). No distinct QT variation was found among the leading SSA components: remaining components (not shown) are primarily in the 1–2.5 year range, with some lower frequency contamination. No significant seasonal variation survived in the "seasonally adjusted" $\delta^{13}C$, although a CO_2 seasonal component was isolated by the joint analysis (not shown).

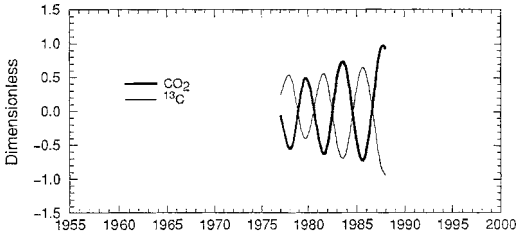

Fig. 12. Bivariate SSA reconstruction of the leading (QQ) mode of shared interannual variability of Mauna Loa CO_2 and the average of seasonally adjusted $\delta^{13}C$ series from Mauna Loa and the South Pole.

The out-of-phase QQ relation between CO_2 and $\delta^{13}C$ is consistent with a terrestrial origin for the QQ variations in CO_2 because terrestrial sources of CO_2 will tend to depress the $\delta^{13}C$ even as they contribute to elevated CO_2 concentrations. In contrast, the QT CO_2 mode is not present among the shared CO_2 and $\delta^{13}C$ variations because this CO_2 mode is dominated by the influence of upwelling variations in the eastern Pacific "source" area on atmospheric CO_2, which does not directly modify atmospheric $\delta^{13}C$.

4.3. CO_2 and NH continental climate

Interannual $\delta^{13}C$ variations thus indicate differing CO_2 sources for the QQ and QT modes, with the QQ mode likely to have mostly terrestrial origins. To investigate these QQ origins further, various NH and continental climate series were compared, using joint SSA, to the Mauna Loa CO_2 series. Results were mixed, however, because continental series tended to exhibit a somewhat different mix of frequencies than either the Mauna Loa CO_2 or tropical SST series.

Fig. 13. (a) Maximum-entropy spectrum of leading PCs from bivariate SSA detrended, deseasonalized Mauna Loa CO_2 series (Fig. 1c) and NH mean land surface-air temperature anomalies (Fig. 3c). (b) Reconstructions of leading components from the bivariate SSA of CO_2 and NH land temperatures for interannual (QQ and QT) time scales. (c) CO_2 and NH land-temperature anomalies, separately band-pass filtered (Kaylor, 1977) with half-power points at 11 and 13 months. (d) Reconstruction of leading components from bivariate SSA of Mauna Loa CO_2 and the area-weighted average of Palmer hydrologic drought indices for United States climate divisions.

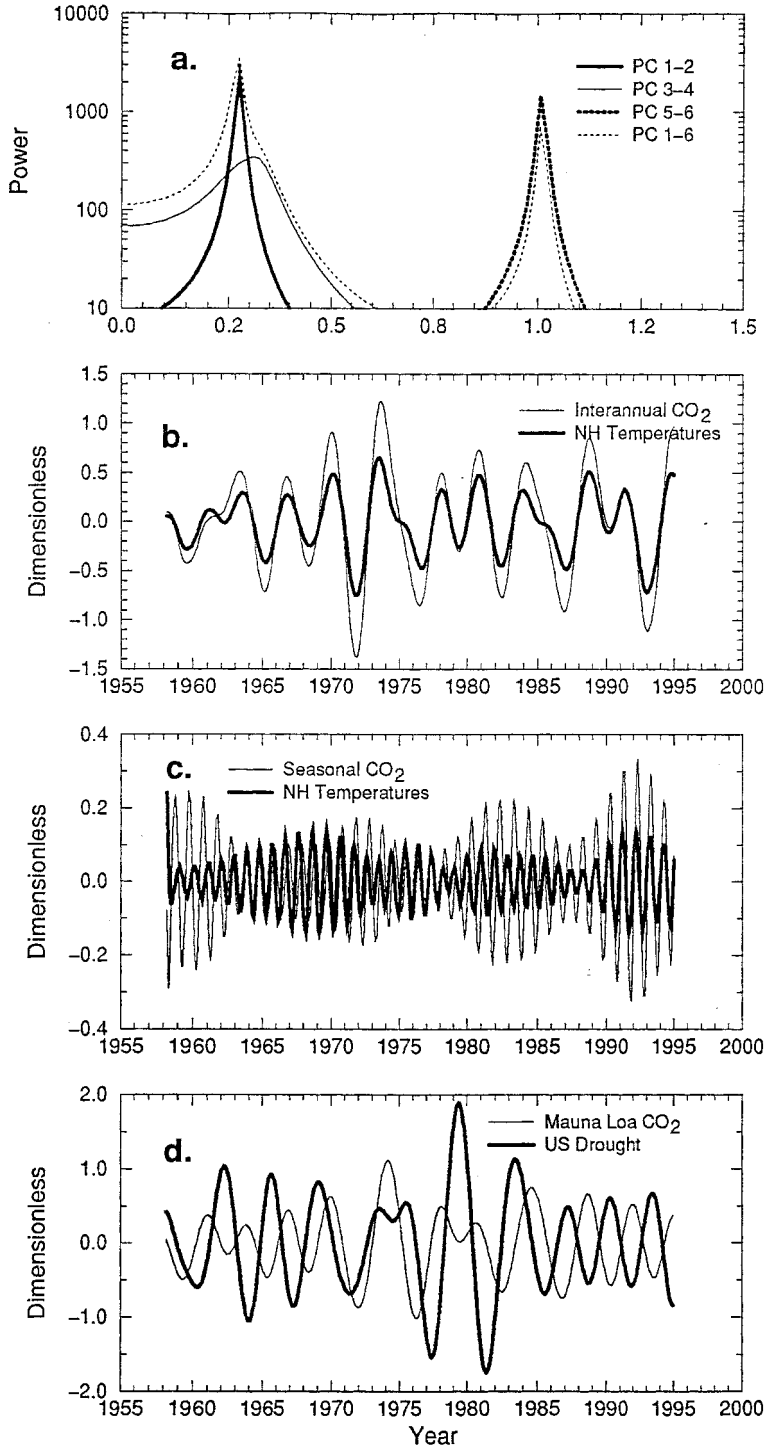
a.
PC 1–2
PC 3–4
PC 5–6
PC 1–6
Power
10000
1000
100
10
0.0
0.2
0.5
0.8
1.0
1.2
1.5
b.
Interannual CO_2
NH Temperatures
Dimensionless
1.5
1.0
0.5
0.0
−0.5
−1.0
−1.5
1955
1960
1965
1970
1975
1980
1985
1990
1995
2000
c.
Seasonal CO_2
NH Temperatures
Dimensionless
0.4
0.2
0.0
−0.2
−0.4
d.
Mauna Loa CO_2
US Drought
Dimensionless
2.0
1.0
0.0
−1.0
−2.0
Year

Fig. 13.

The first two components from a bivariate SSA of Mauna Loa CO_2 and NH-mean land surface-air temperature anomalies capture 15% of the joint variance and are close to the QQ period (Fig. 13a). The somewhat lower frequency (4.5-year period) is probably due to the pair's capturing additional, slightly lower frequencies in the NH land-temperature series (Ghil and Vautard, 1991; Plaut et al., 1995). Components 3 and 4 from the joint analysis capture weak interannual variations with the 3-year period and contribute 8.5% of variance. The 3-year peak in this analysis (Fig. 13a) is notably weaker than the corresponding peak in the joint analysis of tropical SSTs and CO_2 (Fig. 10b).

Reconstructions of each of the four leading components (i.e., both the QQ and QT modes) of this bivariate SSA are summed in Fig. 13b for CO_2 and NH-land temperatures separately. The resulting partial reconstructions of CO_2 and land temperatures are in phase. This provides an indication that NH-land temperatures respond to change in tropical SSTs more or less with the same sign, regardless of whether the signal comes from the upwelling zone of the eastern Pacific or from the rest of the tropical oceans. The relative weakness of the QT signal suggests that the distinctive 3-year SST mode in the eastern tropical Pacific has little direct effect on NH land temperatures (Namias and Cayan, 1984), whereas the QQ mode of the entire tropical belt does have a truly global reach.

Components 5 and 6 capture 7% of the variability of Mauna Loa CO_2 and NH land surface-air temperatures in the form of shared changes in the respective seasonal cycles, as discussed in Section 3.2. These components (not shown) appear to be significant as a distinct pair in a scree plot of SSA eigenvalues and emerge from the bivariate SSA with closely shared phases and amplitudes. As noted for Fig. 5, the large land masses of the NH have experienced changes in the seasonal cycle of temperatures that are temporally similar to, and mostly in phase with, those of the Mauna Loa CO_2 variation (see also Fig. 3). Using a simpler approach, even NH land-mean temperature and Mauna Loa CO_2 series that have been separately band-pass filtered between 11 and 13 months (Fig. 13c) maintain similar amplitude envelopes and, with the notable exception of the early 1980s, remain nearly in phase. Previously, Kuo et al. (1990) demonstrated significant coherence between Mauna Loa CO_2 and NH temperature anomalies in a narrow band centered on the annual cycle by using multitaper methods; their complex demodulation of 1880–1988 NH temperatures, between 0.9 and 1.1 yr^{-1}, included long-term variations of the NH seasonal cycle of temperatures roughly similar to Fig. 3a. The coherent, fairly consistent in-phase relation between CO_2 and NH-land temperatures probably follows from increases (decreases) in release of CO_2 by respiration during winter that are warmer (colder) than normal. Photosynthesis (which also might increase during warmer-than-normal summers and which would sequester CO_2 in the short term) appears to be a more complex function of temperatures and moisture availability (Goulden et al., 1996).

The additional "bulge" in the amplitude envelope of Fig. 13c that occurs around 1970 (relative to the envelope of Fig. 3a) arises because the series analyzed for Fig. 13c have both had their trends and mean seasonal cycles subtracted prior to analysis (as in Fig. 1a), whereas the series analyzed in Fig. 3a had only been detrended. Thus, in Fig. 13c, from about 1965 until about 1975, seasonal variations were smaller than the long-term seasonal cycle and appear as substantial "negative amplitudes" when subtracted from that long-term seasonal cycle. The similarity of the changes in seasonal CO_2 cycle and seasonal land-temperature cycle is striking (especially so in the M-SSA reconstructions) and suggests that, on seasonal time scales, continental climate variations may underlie the observed changes in the seasonal CO_2 cycle, at least at Mauna Loa. Bivariate SSA of the NH land-and-ocean mean temperature series (not shown) does not yield seasonal variations that parallel so closely those found in the univariate SSA of CO_2; instead, we find a shared annual mode that is only intermittently active and that is not well separated from the 3-year signal.

A joint SSA of Mauna Loa CO_2 concentrations and the average of United States divisional Palmer hydrologic drought indices was carried out to investigate the contributions to atmospheric CO_2 of precipitation variability over a representative NH land area. The Palmer hydrologic drought index is essentially a surface balance of moisture fluxes, based on measured precipitation and estimated evaporation; the latter estimate uses observed antecedent precipitation and current temperatures.

When the drought index is positive, wet soil-moisture conditions predominate and terrestrial ecosystems are expected to flourish; when it is negative, dry conditions prevail.

QQ-like variations of CO_2 and Palmer drought indices, but not QT variations, emerged from the joint analysis. The leading four components comprise a mix of frequencies, with dominant periods of 3.6–4.1 years. The sum of these four components (Fig. 13d) does not display a consistent phase relation between CO_2 and the drought index, each of which can lead or lag the other. This variable phasing of CO_2 and drought indices may reflect the complexity of the time lags and interactions between precipitation and temperature anomalies that form the indices. Although soil-moisture conditions presumably play an important role in CO_2 variability, that role apparently is not as simple and amenable to isolation by a linear analysis such as SSA as are the temperature-CO_2 relations. No notable variation of the seasonal cycle was found in the drought index series.

5. Summary and conclusions

The present study has used univariate singular-spectrum analysis (SSA) to isolate seasonal and interannual variations of atmospheric CO_2 concentrations at Mauna Loa Observatory and the South Pole (Figs. 1, 2); bivariate SSA analyses were used to relate these variations to various climate indices, global and regional. The univariate analyses illustrate long-term changes in the amplitude of the seasonal CO_2 cycle that are regional in nature and that, at least at Mauna Loa, follow the low-frequency course of hemispheric mean air temperatures (Fig. 3), as well as the changes in temperature seasonality over Northern Hemisphere (NH) land masses (Figs. 5, 13c). Changes in the phase of the seasonal CO_2 cycle at the South Pole are larger than those at Mauna Loa and mirror hemispheric and global temperature trends (Fig. 4). Recent changes in the seasonal cycle of CO_2 variation at both locations include a hastening of the onset of winter and summer CO_2 sources and sinks, for each hemisphere separately (Figs. 1b, 2b), and a general increase in amplitude of the seasonal CO_2 cycle in both locations.

Univariate SSA also isolates interannual CO_2 variations at both Mauna Loa (Fig. 6) and the South Pole that appear to be consonant with tropical processes (Fig. 7). These interannual variations can be further decomposed into two modes, quasi-quadrennial (QQ) and quasi-triennial (QT). The QQ mode isolated by using joint SSA of CO_2 and tropical SSTs has CO_2 variations that are stronger and in phase with the corresponding SSTs (Fig. 9a). The QQ modes are associated with global temperature variations (Figs. 8 and 11a) and their CO_2 expression is probably a response to terrestrial ecosystem changes associated with temperature variations on global scales. In particular, as temperatures increase, respiration increases in terrestrial ecosystems and the balance between the CO_2 sources and sinks is shifted temporarily towards the sources (see Section 1). If the temperature increases are large enough and widespread enough, regional and global CO_2 concentrations increase.

Bivariate SSAs of CO_2 and various tropical climate indices (including tropical-belt sea-surface temperatures (SSTs)) also isolates a shared QT mode in which CO_2 and SST participation are 180° out-of-phase (Fig. 9b). This mode appears to derive from the roughly 3-year fluctuations of SST in the eastern Tropical Pacific (Figs. 8 and 11b). A simple explanation for this out-of-phase relation might be that anomalously weak upwelling of cool, CO_2-rich ocean water in the eastern tropical Pacific reduces CO_2 outgassing there, decreases atmospheric CO_2, and increases tropical SST during El Niño events; the opposite occurs during La Niña episodes. These changes in tropical ocean upwelling are evidently large enough to be felt nearly globally in CO_2 levels, whereas the SST and climate effects are much more regional.

Joint SSA of Mauna Loa CO_2 with a seasonally adjusted atmospheric $\delta^{13}C$ series yields strong QQ components that are out of phase with each other (Fig. 12). No variations with a distinct 3-year period were found. These amplitudes and phase relations support the hypothesis that QT variations of CO_2 at Mauna Loa and the South Pole are dominated by marine influences on atmospheric CO_2 concentrations, presumably following the relatively localized upwelling variations in the eastern tropical Pacific. Although upwelling variations undoubtedly contribute to the QQ variations in CO_2, the latter are dominated by the effects of the near-global QQ temperature variations on terrestrial climate, ecosystems response and, through them, CO_2 concentrations.

Joint SSA of Mauna Loa CO_2 with NH-land mean air temperature anomalies isolated shared variations with annual, QQ, and much weaker QT periods. CO_2 and continental NH temperature variations appear to be generally in phase in all three narrow frequency bands considered (Figs. 13b, c). The interannual variations in continental temperature seasonality shared with Mauna Loa CO_2 are similar and in phase, to a remarkable extent (Fig. 13c). The results of bivariate SSA also suggest a northern continental source for the CO_2 seasonality changes.

Analysis of Palmer drought indices — as surrogates for soil moisture and hence ecosystem vigor — in the United States revealed only QQ-like modes in common with CO_2. Presumably, the climatic effects of the QQ tropical and global ocean climate mode on North American climate and ecosystems are considerably stronger than the effects of the more localized QT, eastern tropical Pacific mode. The QQ drought-index variations shared with CO_2 do not exhibit a consistent phase relation between the two time series. Indeed, correlations between temperatures, precipitation, tropical climate indices, and drought indices across the United States (not shown) revealed a complex interleaving of regional temperature and precipitation influences that determine the drought indices for specific seasons on interannual time scales.

To summarize, univariate and bivariate SSA has helped isolate and reconstruct annual, QT, and QQ modes of CO_2 variability at Mauna Loa and the South Pole. The interannual CO_2 variations are strongly linked with variations of tropical SSTs: ocean upwelling in the eastern tropical Pacific dominates the QT mode, and global climate and biosphere responses to tropical-belt SST variations dominate the QQ mode. A substantial effect of NH terrestrial climate on CO_2 concentrations has also been identified by the bivariate SSA and by simple correlation analyses with atmospheric $^{13}C/^{12}C$ isotopic ratios, continental NH surface-air temperatures, and North American drought indices. Marine-upwelling variability appears to directly influence the QT mode of atmospheric CO_2 concentrations and is presumably present also in the QQ mode. The QQ climate mode, however, involves temperature and precipitation variations over much broader areas that include the large NH land masses. The responses of terrestrial ecosystems to these farflung QQ climate variations dominate over QQ upwelling effects in the interannual CO_2 variations at both Mauna Loa and the South Pole.

6. Acknowledgements

This work benefited greatly from access to the U. S. Department of Energy's (DOE's) Carbon Dioxide Information Analysis Center's various data archives, from climatic time series provided by D. R. Cayan at the Scripps Institution of Oceanography (SIO) and J. Eischeid of NOAA's Climate Data Center, and from isotopic time series provided by P. Tans and M. Trolier of NOAA's Climate Monitoring and Diagnostics Laboratory. Our ongoing interactions with the SSA Group and Toolkit makers greatly facilitated our analysis of all these time series. Comments from and discussions with D. R. Cayan, with V. Moron from the Université de Bourgogne, Dijon, and with C. Penland, M. Hoerling, and Klaus Weickmann of the NOAA Climate Diagnostics Center contributed also. E. Bainto at SIO's Climate Research Division provided graphical support. MD's work was supported by the U. S. Geological Survey's Global Change Hydrology Program. MG's research was supported at UCLA by NSF grant ATM95–23787, and at the Ecole Normale Supérieure by a Elf-Aquitaine/CNRS Chair of the Académie des Sciences, Paris. This is publication no. 4893 of UCLA's Institute of Geophysics and Planetary Physics.

REFERENCES

Allen, M. R. 1992. *Interactions between the atmosphere and oceans on time scales of weeks to years*. PhD thesis, St. John's College, Oxford, 203 p.

Allen, M. R., and Smith, L. A. 1996. Monte Carlo SSA: Detecting irregular oscillations in the presence of colored noise. *J. Clim.* **9**, 3373–3404.

Angell, J. K. 1990. Variation in global tropospheric temperature after adjustment for the El Niño influence, 1958–89. *Geophys. Res. Lett.* **17**, 1093–1096.

Bacastow, R. B., Keeling, C. D. and Whorf, T. P. 1985. Seasonal amplitude increase in atmospheric CO_2 concentration at Mauna Loa, Hawaii, 1959–82. *J. Geophys. Res.* **90**, 10 529–10 540.

Broomhead, D. S. and King, G. 1986. Extracting qualit-

ative dynamics from experimental data. *Physica D* **20**, 217–236.

Chang, P., Wang, B. and Link, J. 1994. Interactions between the seasonal cycle and the Southern Oscillation–Frequency entrainment and chaos in a coupled ocean-atmosphere model. *Geophys. Res. Lett.* **21**, 2817–2820.

Ciais, P., Tans, P. P., Trolier, M., White, J. W. C. and Francey, R. J. 1995. A large Northern Hemisphere terrestrial CO_2 sink indicated by $^{13}C/^{12}C$ ratio of atmospheric CO_2. *Science* **269**, 1098–1102.

Colebrook, J. M. 1978. Continuous plankton records–Zooplankton and environment, northeast Atlantic and North Sea, 1948–1975. *Oceanol. Acta* **1**, 9–23.

Conway, T. J., Tans, P. P., Waterman, L. S., Thoning, K. W., Kitzis, D. R., Masarie, K. A. and Zhang, N. 1994. Evidence for interannual variability of the carbon cycle from the National Oceanic and Atmospheric Administration/Climate Monitoring and Diagnostics Laboratory global air sampling network. *J. Geophys. Res.* **99**, 22831–22855.

Dettinger, M. D., Ghil, M. and Keppenne, C. L. 1995a. Interannual and interdecadal variability of United States surface-air temperatures, 1910–1987. *Climatic Change* **31**, 35–66.

Dettinger, M. D., Ghil, M., Strong, C. M., Weibel, W. and Yiou, P. 1995b. Software expedites singular-spectrum analysis of noisy time series. *Eos, Trans. AGU* **76**, 12, 14, 21.

Fraedrich, K. 1986. Estimating the dimensions of weather and climate attractors. *J. Atmos. Sci.* **43**, 419–432.

Francey, R. J., Tans, P. P., Allison, C. E., Enting, I. G., White, J. W. C. and Trolier, M. 1995. Changes in oceanic and terrestrial carbon uptake since 1982. *Nature* **373**, 326–330.

Ghil, M. and Vautard, R. 1991. Interdecadal oscillations and the warming trend in global temperature time series. *Nature* **350**, 324–327.

Ghil, M. and Yiou, P. 1996. Spectral methods: What they can and cannot do for climatic time series. In: *Decadal climate variability: Dynamics and predictability* (D. Anderson Willebrand, eds.). Elsevier, pp. 445–482

Goulden, M. L., Munger, J. W., Fan, S. M., Daube, B. C., and Wofsy, S. C. 1996. Exchange of carbon dioxide by a deciduous forest: Response to interannual climate variability. *Science* **271**, 1576–1578.

Jiang, N., Neelin, D. and Ghil, M. 1995. Quasi-quadrennial and quasi-biennial variability in the equatorial Pacific. *Clim. Dyn.* **12**, 101–112.

Jin, F. F., Neelin, J. D. and Ghil, M. 1994. El Niño on the Devil's staircase: Annual subharmonic steps to chaos. *Science* **264,** 70–72.

Jones, P. D., Raper, S. C. B., Bradley, R. S., Diaz, H. F., Kelly, P. M. and Wigley, T. M. L. 1986a. Northern Hemisphere surface air temperature variations: 1851–1984. *J. Climate Appl. Meteorol.* **25**, 161–79.

Jones, P. D., Raper, S. C. B. and Wigley, T. M. L. 1986b. Southern Hemisphere surface air temperature variations: 1851–1984. *J. Climate Appl. Meteorol.* **25**, 1213–1230.

Jones, P. D., Wigley, T. M. L. and Wright, P. B. 1986c. Global temperature variations between 1861 and 1984. *Nature* **322**, 430–434.

Karl, T. R., Jones, P. D. and Knight, R. W. 1996. Testing for bias in the climate record. *Science* **271**, 1879–1880.

Kaylor, R. E. 1977. *Filtering and decimation of digital time series.* Univ. of Maryland, Dept. of Meterology Tech. Note BN850 (Engineering and Physical Sciences Library, Univ. of Maryland), 14 p.

Keeling, C. D. and Whorf, T. P. 1994. Atmospheric CO_2 records from sites in the SIO air sampling network. In: *Trends '93: A compendium of data on global change* (eds. T. A. Boden, Kaiser, D. P., Sepanski, R. J. and Stoss, F. W.). ORNL/CDIAC-65. Carbon Dioxide Information Analysis Center, Oak Ridge National Laboratory, Oak Ridge, Tenn., pp. 16–26.

Keeling, C. D., Bacastow, R. B., Bainbridge, A. E., Ekdahl, C. E., Jr., Guenther, P. R., Waterman, L. S. and Chin, J. F. S. 1976. Atmospheric carbon dioxide variations at Mauna Loa observatory, Hawaii. *Tellus* **28**, 538–551.

Keeling, C. D., Bacastow, R. B. and Whorf, T. P. 1982. Measurements of the concentrations of carbon dioxide at Mauna Loa observatory, Hawaii. In: *Carbon dioxide review: 1982* (ed. C. Clark). Oxford University Press, New York, 377–385.

Keeling, C. D., Bacastow, R. B., Carter, A. F., Piper, S. C., Whorf, T. P., Heimann, M., Mook, W. G. and Roeloffzen, H. 1989. A three-dimensional model of atmospheric CO_2 transport based on observed winds: 1. Analysis of observational data. In: *Aspects of climate variability in the Pacific and the Western Americas* (ed. D. H. Peterson). AGU Geophysical Monograph 55, 165–236.

Keeling, C. D., Chin, J. F. S. and Whorf, T. P. 1996. Increased activity of northern vegetation inferred from atmospheric CO_2 measurements. *Nature* **382**, 146–149.

Keeling, C. D., Whorf, T. P., Wahlen, M. and van der Plicht, J. 1995. Interannual extremes in the rate of rise of atmospheric carbon dioxide since 1980. *Nature* **375**, 666–670.

Keppenne, C. L. and Ghil, M. 1992. Adaptive spectral analysis and prediction of the Southern Oscillation Index. *J. Geophys. Res.* **97**, 20 449–20 554.

Knorr, W. and Heimann, M. 1995. Impact of drought stress and other factors on seasonal land biosphere CO2 exchange studied through an atmospheric tracer transport model. *Tellus* **47B**, 471–489.

Kuo, C., Lindberg, C. and Thomson, D. J. 1990. Coherence established between atmospheric carbon dioxide and global temperature. *Nature* **343**, 709–714.

Lambert, G., Monfray, P., Ardouin, B., Bonsang, G., Gaudry, A., Kazan, V. and Polian, G. 1995. Year-to-year changes in atmospheric CO_2. *Tellus* **47B**, 53–55.

Latif, M., Sterl, A., Maier-Reimer, E. and Junge, M. M. 1993. Structure and predictability of the El Niño/Southern Oscillation phenomenon in a coupled ocean-

atmosphere general circulation model. *J. Clim.* **6**, 700–708.

Mann, M. E. and Park, J. 1994. Global scale modes of surface temperature variability on interannual to century timescales. *J. Geophys. Res.* **99**, 25 819–25 933.

Mann, M. E. and Park, J. 1996. Greenhouse warming and changes in the seasonal cycle of temperature: Model versus observations. *Geophys. Res. Lett.* **23**, 1111–1114.

Meyers, S. D. and O'Brien, J. J. 1995. Pacific Ocean influences atmospheric carbon dioxide. *Eos, Trans. AGU* **76**, 533, 537.

Moron, V., Vautard, R. and Ghil, M. 1997. Trends, interdecadal and interannual oscillations in the global sea-surface temperature. *Clim. Dyn.* in press.

Murray, J. W., Barber, R. T., Roman, M. R., Bacon, M. P., and Feely, R. A. 1994. Physical and biological controls on carbon cycling in the equatorial Pacific: US JGOFS EqPac process study. *Science* **266**, 58–65.

Myneni, R. B., Keeling, C. D. and Nemani, R. R. 1997. Increased plant growth in the northern high latitudes from 1981 to 1991. *Nature* **386**, 698–701.

Namias, J. and Cayan, D. R. 1984. El Niño: Implications for forecasting. *Oceanus* **27**, 41–47.

Nemry, B., Francois, L. Warnant, P. Roloinet F and Gerard, J.-C. 1996. The seasonality of the CO_2 exchange between the atmosphere and the land biosphere–A study with a global mechanistic vegetation model. *J. Geophys. Res.* **101**, 7111–7125.

Okamoto, K., Tanimoto, S. and Okano, K. 1995. Statistical analysis of the increase in atmospheric CO_2 concentrations and its relation to the possible existence of CO_2 fertilization on a global scale. *Tellus* **47B**, 206–211.

Parker, D. E., Folland, C. K., Bevan, A., Ward, M. N., Jackson, M., and Maskell, K. 1995. Marine surface data for analysis of climatic fluctuations on interannual to century timescales. In: *Natural climate variability on decade-to-century time scales* (D. G. Martinson et al., eds.). National Academy Press, Washington, DC, pp. 241–250.

Plaut, G. and Vautard, R. 1995. Spells of low-frequency oscillations and weather regimes in the northern hemisphere. *J. Atmos. Sciences* **51**, 210–236.

Press, W. H., Flannery, B. P., Teukolsky, S. A. and Vetterling, W. T. 1989. *Numerical recipes — the art of scientific computing* (FORTRAN Version). Cambridge Univ. Press, New York, 702 pp.

Rasmusson, E. M., Wang, X. and Ropelewski, C. 1990. The biennial component of ENSO variability. *J. Mar. Syst.* **1**, 71–96.

Robertson, A. W. 1996. Interdecadal variability over the North Pacific in a multi-century climate simulation. *Clim. Dyn.* **12**, 227–242.

Robertson, A. W., Ma, C. C., Ghil, M. and Mechoso, C. R. 1995. Simulation of the tropical Pacific climate with a coupled ocean-atmosphere general circulation model. Part II: Interannual variability. *J. Clim.* **8**, 1199–1216.

Ropelewski, C. F. and Halpert, M. S. 1987. Global and regional scale precipitation patterns associated with the El Niño/Southern Oscillation. *Monthly Wea. Rev.* **115**, 1606–1626.

Sarmiento, J. L. 1993. Atmospheric CO_2 stalled. *Nature* **365**, 697–698.

Siegenthaler, U. 1990. El Niño and atmospheric CO_2. *Nature* **345**, 295–296.

Siegenthaler, U. and Sarmiento J. L. 1993. Atmospheric carbon dioxide and the ocean. *Nature* **365**, 119–125.

Spencer, R. W. and Christie, J. R. 1992. Precision and radiosonde validation of satellite gridpoint temperature anomalies. Part II: A tropospheric retrieval and trends during 1979–90. *J. Clim.* **5**, 858–866.

Suarez, M. J. and Schopf, P. S. 1988. A delayed action oscillator for ENSO. *J. Atmos. Sci.* **45**, 3283–3287.

Sundquist, E. T. 1993. The global carbon dioxide budget. *Science* **259**, 934–941.

Thomson, D. J. 1995. The seasons, global temperatures, and precession. *Science* **268**, 59–68.

Thomson, D. J. 1996. Testing for bias in the climate record. *Science* **271**, 1881–1883.

Trumbore, S. E., Chadwick, O. A. and Amundson, R. 1996. Rapid exchange between soil carbon and atmospheric carbon dioxide driven by temperature change. *Science* **272**, 393–396.

Tziperman, E., Stone, L., Cane, M. A. and Jarosh, H. 1994. El Niño chaos: Overlapping of resonances between the seasonal cycle and the Pacific ocean-atmosphere oscillator. *Science* **264**, 72–74.

Unal, Y. S. and Ghil, M. 1995. Interannual and interdecadal oscillation patterns in sea level. *Clim. Dyn.* **18**, 255–278.

Vautard, R. and Ghil, M. 1989. Singular spectrum analysis in nonlinear dynamics, with applications to paleoclimatic time series. *Physica D* **35**, 395–424.

Vautard, R., Yiou, P. and Ghil, M. 1992. Singular-spectrum analysis: A toolkit for short, noisy chaotic signals. *Physica D* **58**, 95–126.

White, O. R., Mende, W. and Beer, J. 1996. Testing for bias in the climate record. *Science* **271**, 1880–1881.

WMO 1984. *Summary Report on the Status of the WMO background air pollution monitoring network as at May 1984*. World Meteorological Organization Technical Document WMO/TD 13. Geneva, 21 pp.